Supporting Information

One-Step Sintering Synthesis of Robust Self-Supported MoSe2/Ni3Se2 Heterostructure Electrode for Efficient Hydrogen Evolution at High Current Density

Manman Cui, Yi Zhang, Bin, Zhang*, Yang Zhao*, Wenjing Gu, Lu Yang, Shizhong Wei, and Zhanling Zhang*

M. Cui, Dr. B. Zhang, Dr. Y. Zhao, W. Gu, Dr. Lu Yang, Prof. S. Wei, Prof. Z. Zhang

School of Materials Science and Engineering, Henan University of Science and Technology, Luoyang 471003, China

Y. Zhang

Tianjin Plannano Energy Technologies Company Ltd., 8 Gaoying Road, Tianjin 300350, China.

E-mail of corresponding authors:

Bin Zhang: zhangbin15@tsinghua.org.cn

Yang Zhao: gloryfire@126.com

Zhanling Zhang: zzling@haust.edu.cn

Experimental section

Materials

Commercial Mo powder with average size of ~200 nm, Ni powder with average size of ~2.5 μm and Se powder with average size of ~500 nm were used as raw materials.

Synthesis of self-supported electrodes

$MoSe_2/Ni_3Se_2$ heterostructure self-supported electrodes were synthesized by simple one-step sintering method. First, the certain masses of Mo, Ni and Se powders were thoroughly mixed to ensure homogeneity. Then, the mixture was pressed into tablet in a tablet press machine using a custom-made mold (Fig. S1). Finally, the tablet was sintered in a tube furnace under vacuum conditions to obtain $MoSe_2/Ni_3Se_2$ electrode. The electrodes prepared by fixing the mass of Mo (500 mg), Ni (1500 mg) and Se (400 mg) powders with different sintering temperatures (750, 800, 850, and 900 °C) are denoted as $MoSe_2/Ni_3Se_2$-X, where X represents the sintering temperature. The $MoSe_2/Ni_3Se_2$-800 electrodes with different masses of Se (200 mg, 300 mg, and 500 mg) were labeled as $MoSe_2/Ni_3Se_2$-800-1, $MoSe_2/Ni_3Se_2$-800-2, and $MoSe_2/Ni_3Se_2$-800-3. The electrodes prepared by fixing the mass of Mo (500 mg), Ni (1500 mg), Se (400 mg) powders and the sintering temperature (800 °C) with different holding times (90 and 150 min) were noted as $MoSe_2/Ni_3Se_2$-800-90 and $MoSe_2/Ni_3Se_2$-800-150.

The MoS_2/Ni_3S_2-700 electrode was synthesized using the same one-step sintering process, with a sintering temperature of 700 °C and a sintering time of 2 h, using Ni (1.5g), Mo (500mg), and S (150mg) powder as raw materials.

Characterization

The X-ray diffraction (XRD) of the samples were obtained on a Bruker D8 Advance diffractometer with a Cu-targeted Ka-signal emission source. The morphological features and elemental distribution were characterized using field emission scanning electron microscopy (SEM) (ZEISS Sigma 300) and transmission electron microscopy (TEM) (FEI Talos F200X G2). Raman spectroscopy (Lab RAMHR800) and X-ray photoelectron spectrometer (XPS) (Thermo Scientific K-Alpha) characterized the surface composition and electronic states.

Electrochemical measurement

All electrochemical experiments were performed on a Biologic VSP electrochemical workstation using a standard three-electrode system in alkaline medium (1.0 M KOH). The prepared electrode was directly used as working electrode, graphite rod as counter electrode and Hg/HgO electrode as reference electrode. The catalytic activity of $MoSe_2/Ni_3Se_2$ electrode for HER was assessed using linear scanning voltammetry

(LSV) at a scan rate of 5 mV s^{-1}. CV curves were gathered at 10-100 mV s^{-1} scan rates to evaluate the capacitive currents. Then the electrochemical double layer capacitance (C_{dl}) was calculated. The electrochemical impedance spectra (EIS) were obtained at various overpotentials including 60, 90, 120, and 150 mV, within a frequency range spanning from 1.0 MHz to 10.0 mHz, and with an amplitude set at 10 mV. For accurate measurement, all recorded potentials were subsequently calibrated to the reversible hydrogen electrode (RHE) utilizing the following equation: $E_{RHE} = E_{Hg/HgO} + E + 0.059\,pH$.Chronoamperometric (i-t) tests were performed at different current densities of 400, 600, 800 and 1000 mA cm^{-2} for 12 h to verify stability of the $MoSe_2/Ni_3Se_2$-800 electrode. The long-term stability was tested at current density of 800 mA cm^{-2}.

Fig. S1. Photos of the custom-made mold of (a) Individual parts separated and (b) combination mold.

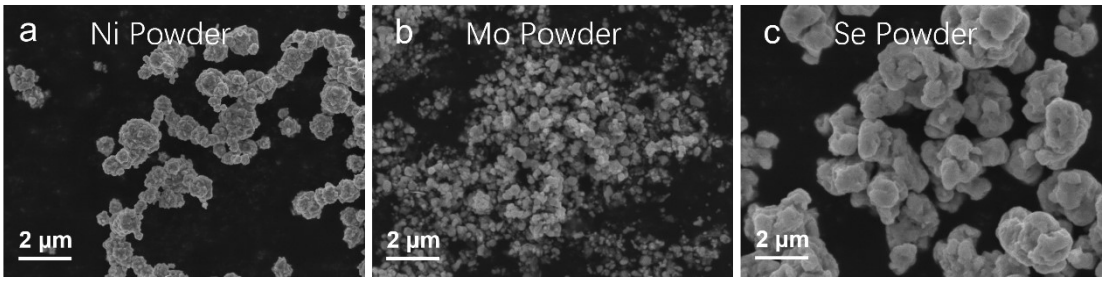

Fig. S2. SEM images of (a) Ni, (b) Mo, and (c) Se powder.

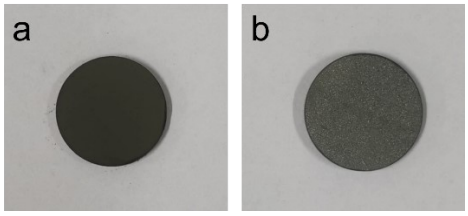

Fig. S3. Photos of the electrodes before and after catalyst sintering

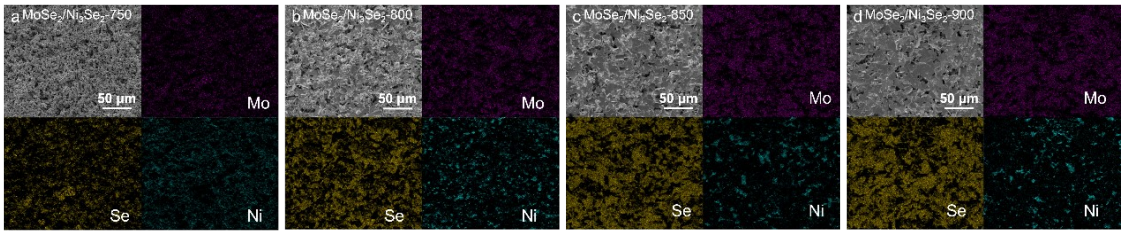

Fig. S4. EDS mappings of (a) $MoSe_2/Ni_3Se_2$-750, (b) $MoSe_2/Ni_3Se_2$-800, (c) $MoSe_2/Ni_3Se_2$-850, and (d) $MoSe_2/Ni_3Se_2$-900.

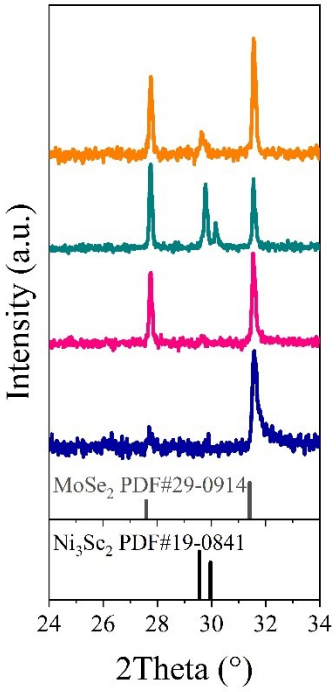

Fig. S5. Enlarging the light blue boxed area in Fig. 3a

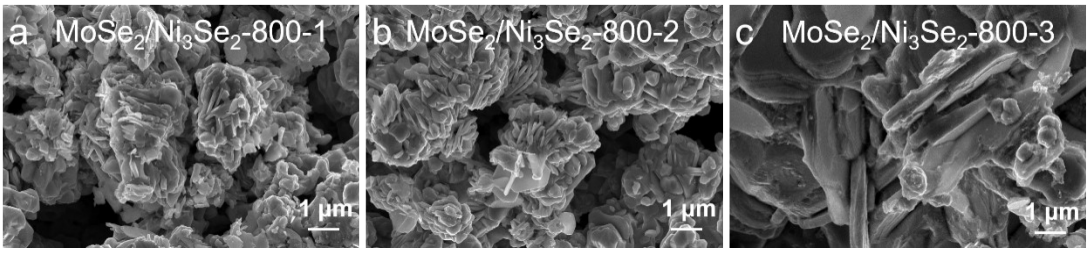

Fig. S6. SEM images of (a) $MoSe_2/Ni_3Se_2$-800-1, (b) $MoSe_2/Ni_3Se_2$-800-2, and (c) $MoSe_2/Ni_3Se_2$-800-3 electrodes.

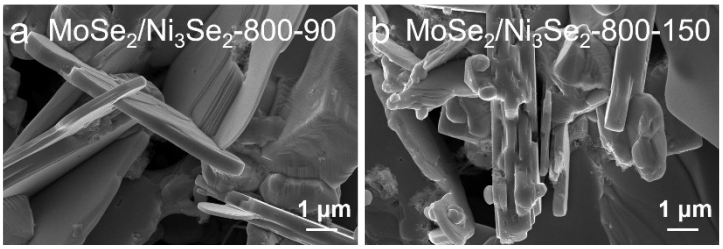

Fig. S7. SEM images of (a) $MoSe_2/Ni_3Se_2$-800-90 and (b) $MoSe_2/Ni_3Se_2$-800-150 electrodes.

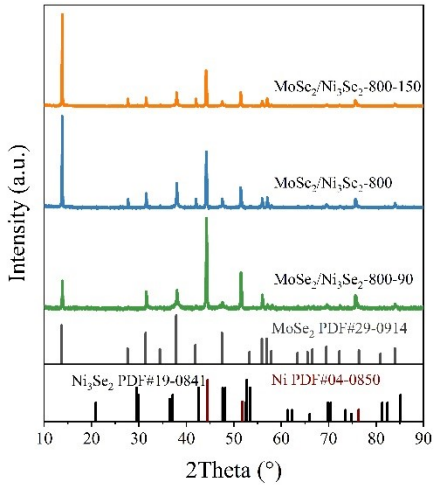

Fig. S8. XRD patterns of $MoSe_2/Ni_3Se_2$-800-90, $MoSe_2/Ni_3Se_2$-800 and $MoSe_2/Ni_3Se_2$-800-150 electrodes.

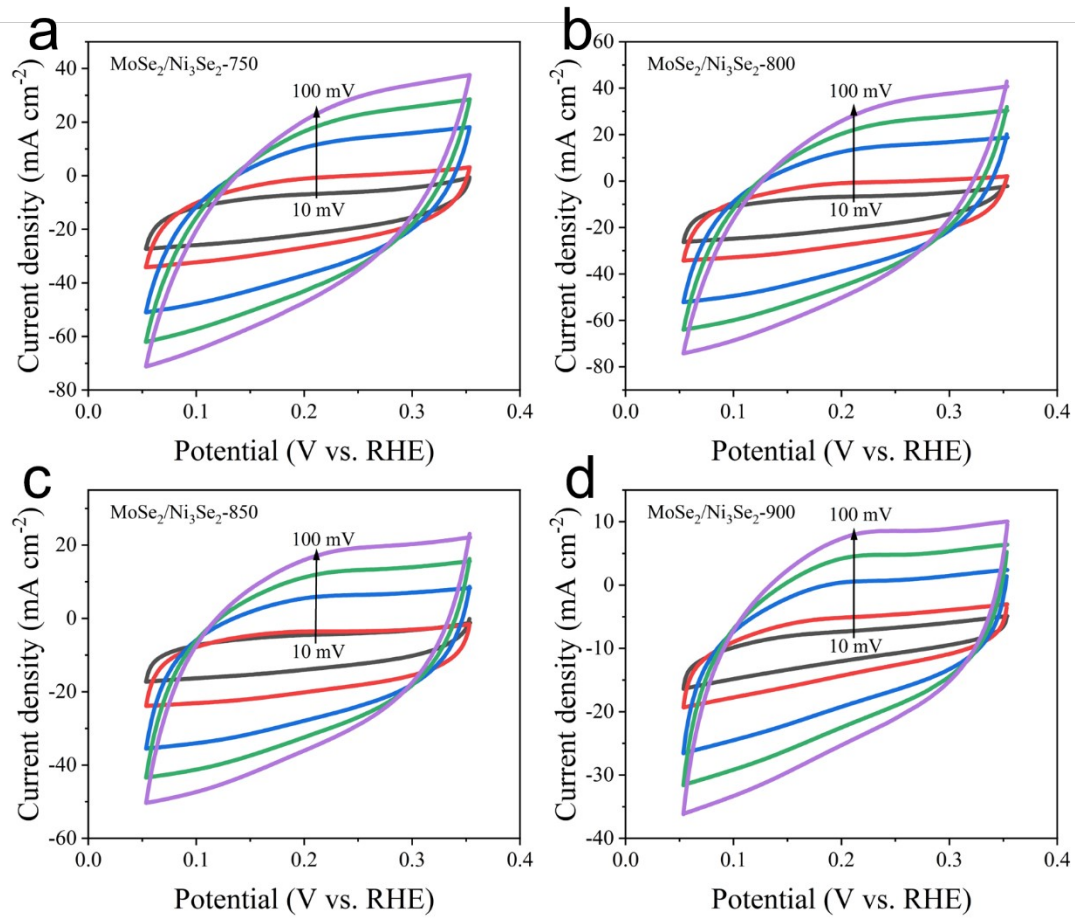

Fig. S9. Cyclic voltammograms (CVs) of (a) $MoSe_2/Ni_3Se_2$-750, (b) $MoSe_2/Ni_3Se_2$-800, (c) $MoSe_2/Ni_3Se_2$-850, and (d) $MoSe_2/Ni_3Se_2$-900 electrodes.

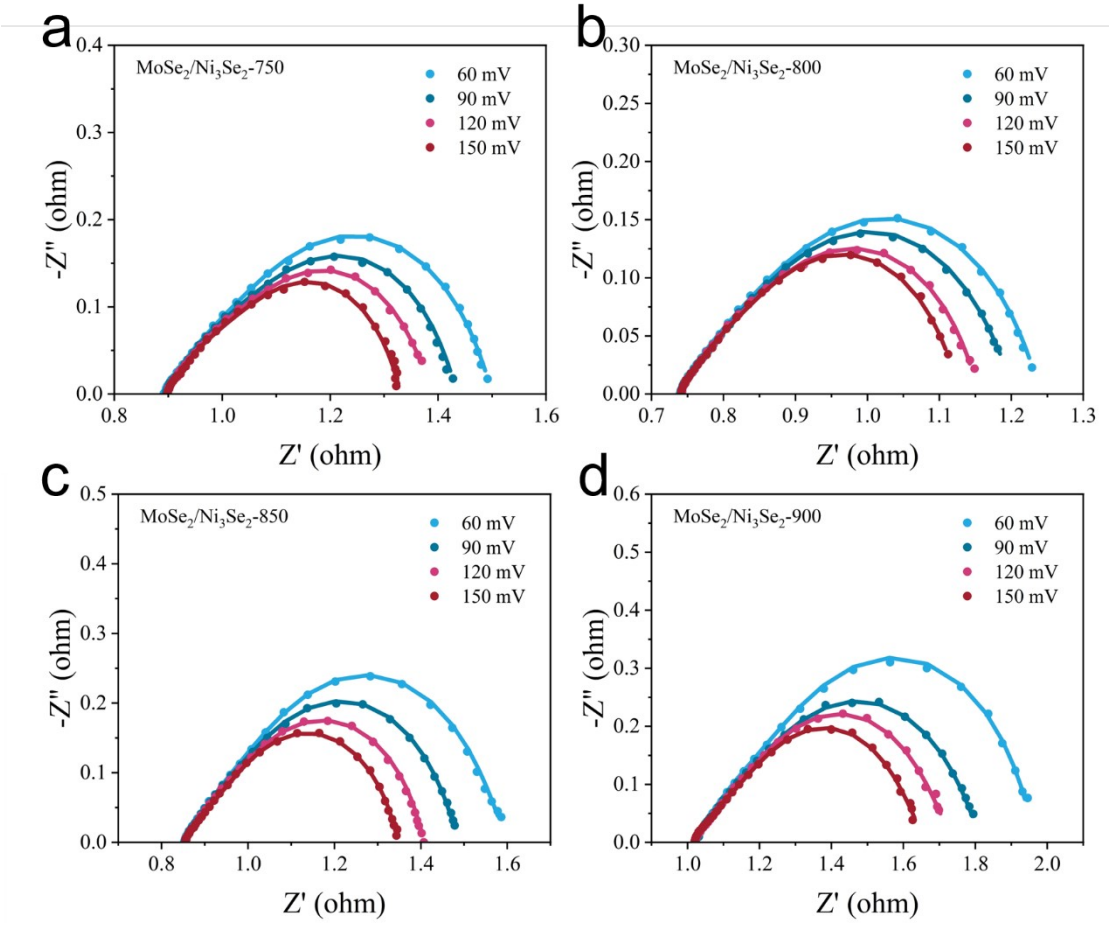

Fig. S10. Nyquist plots of (a) $MoSe_2/Ni_3Se_2$-750, (b) $MoSe_2/Ni_3Se_2$-800, (c) $MoSe_2/Ni_3Se_2$-850, and (d) $MoSe_2/Ni_3Se_2$-900 electrodes.

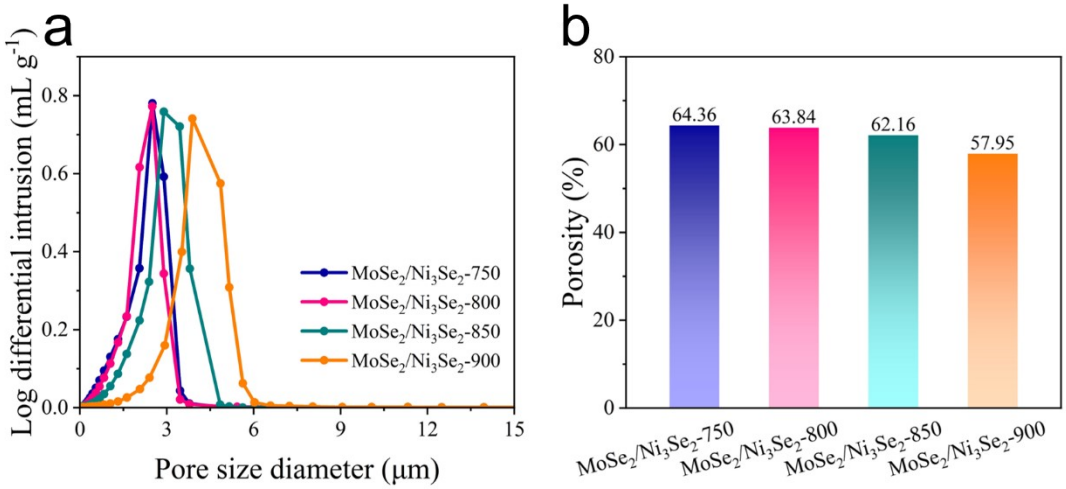

Fig. S11. (a) Pore size distribution and (b) Porosity of $MoSe_2/Ni_3Se_2$-750, $MoSe_2/Ni_3Se_2$-800, $MoSe_2/Ni_3Se_2$-850, and $MoSe_2/Ni_3Se_2$-900 electrodes.

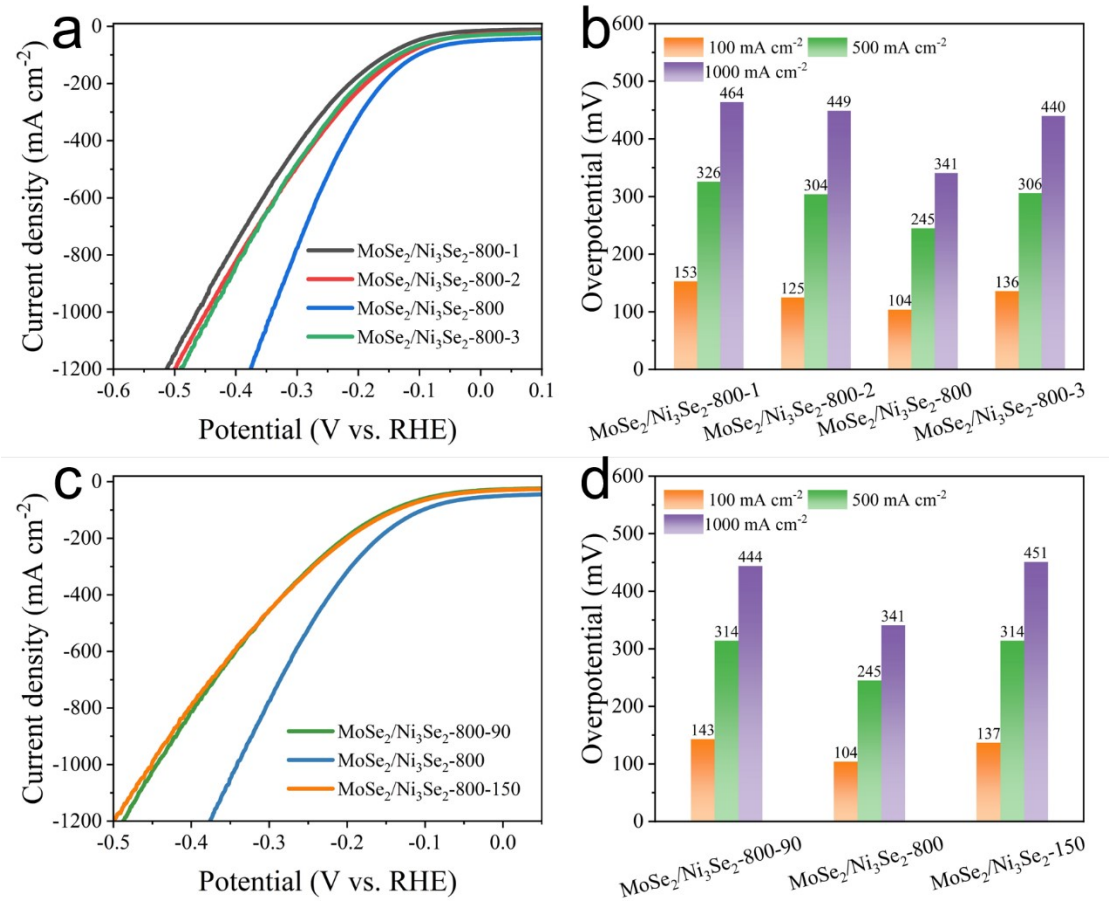

Fig. S12. (a) Comparison of Polarization curves of $MoSe_2/Ni_3Se_2$-800-1, $MoSe_2/Ni_3Se_2$-800-2, $MoSe_2/Ni_3Se_2$-800, and $MoSe_2/Ni_3Se_2$-800-3. (b) Comparison of overpotentials at 100 mA cm^{-2}, 500 mA cm^{-2}, and 1000 mA cm^{-2} in (a). (c) Comparison of Polarization curves of $MoSe_2/Ni_3Se_2$-800-90, $MoSe_2/Ni_3Se_2$-800, and $MoSe_2/Ni_3Se_2$-800-150. (d) Comparison of overpotentials at 100 mA cm^{-2}, 500 mA cm^{-2}, and 1000 mA cm^{-2} in (c).

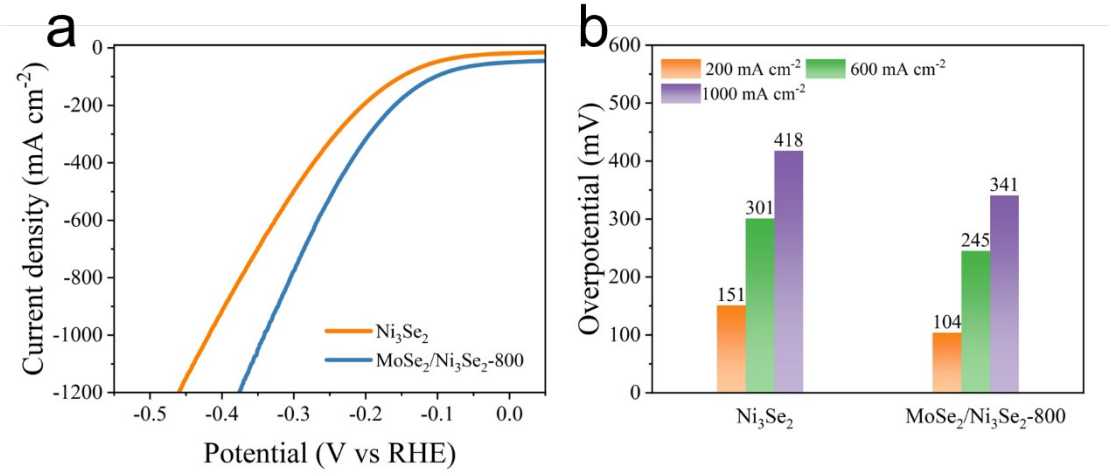

Fig. S13. (a) Comparison of Polarization curves of Ni_3Se_2-Ni600 and $MoSe_2/Ni_3Se_2$-800. (b) Comparison of overpotentials at 100 mA cm^{-2}, 500 mA cm^{-2}, and 1000 mA cm^{-2} in (a).

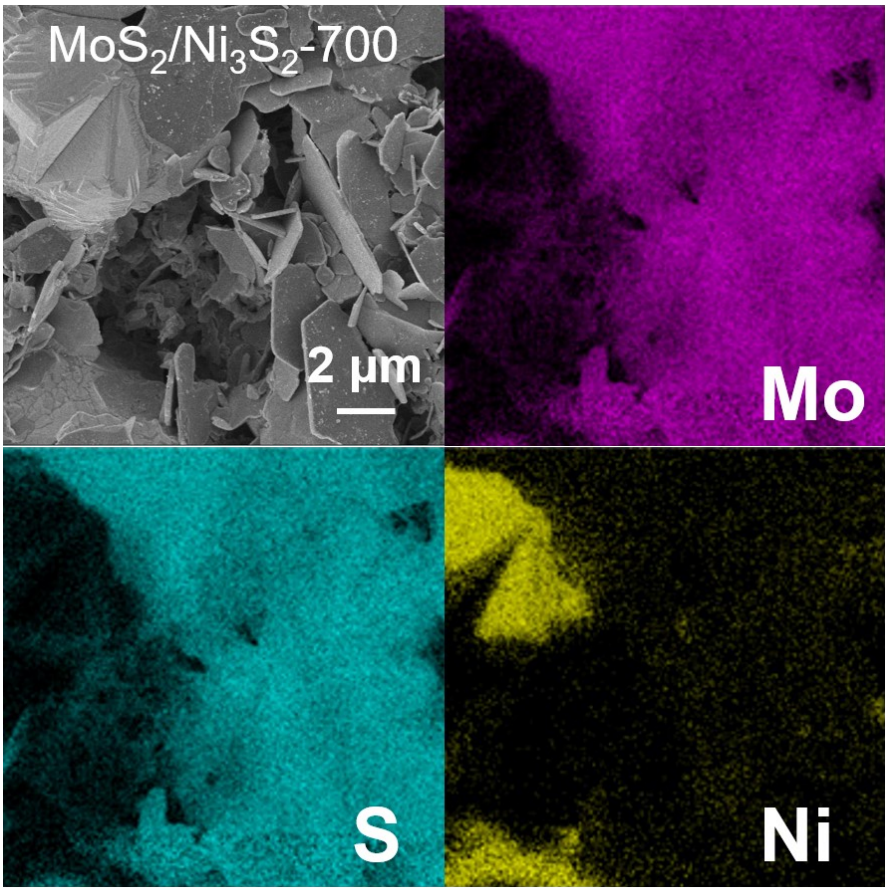

Fig. S14. SEM image and EDS mappings of MoS_2/Ni_3S_2-700.

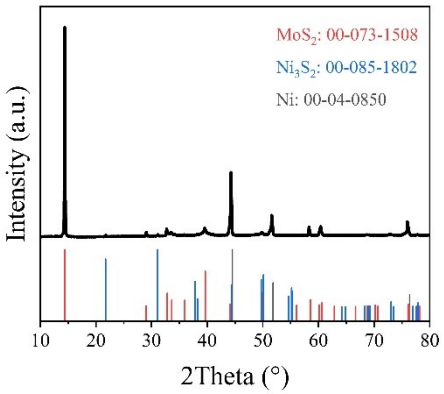

Fig. S15. XRD pattern of MoS_2/Ni_3S_2-700.

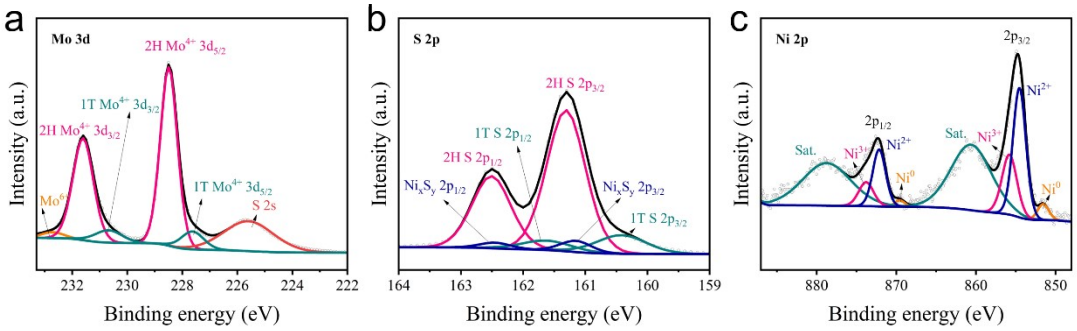

Fig. S16. XPS spectra of (a) Mo 3d, (b) S 2p, (c) Ni 2p of MoS_2/Ni_3S_2-700.

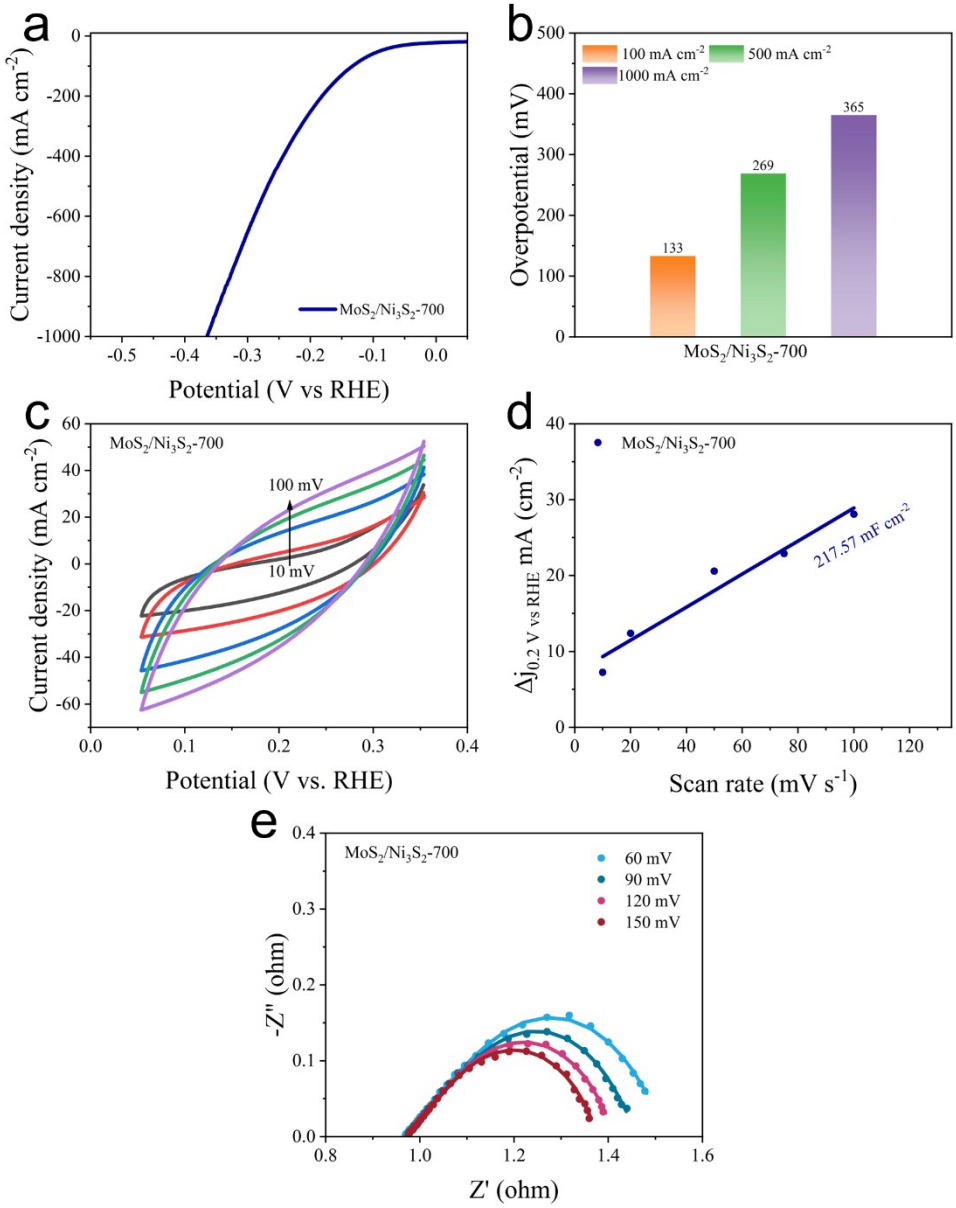

Fig. S17. (a) Polarization curve of MoS_2/Ni_3S_2-700. (b) Comparison of overpotentials at 100 mA cm^{-2}, 500 mA cm^{-2}, and 1000 mA cm^{-2} in (a). (c) Calculated electrochemical double-layer capacitance (C_{dl}) of MoS_2/Ni_3S_2-700 treated with different CV scan rates. (d) Nyquist plots of MoS_2/Ni_3S_2-700.

Table S1. Simulated equivalent circuit data.

Overpotential（mV）	90
$MoSe_2/Ni_3Se_2$-750 Rct（Ω cm^{-2}）	0.26
$MoSe_2/Ni_3Se_2$-800 Rct（Ω cm^{-2}）	0.24
$MoSe_2/Ni_3Se_2$-850 Rct（Ω cm^{-2}）	0.35
$MoSe_2/Ni_3Se_2$-900 Rct（Ω cm^{-2}）	0.41

Table S2. Comparison of the stability of our $Mose_2/Ni_3Se_2$-800 electrode with other reported electrocatalysts.

electrocatalysts	Stability	Ref.
Ni-NiO-Pt	75h@500 mA cm^{-2}	[1]
Ni_3S_2/Cr_2S_3/NF	50h@500 mA cm^{-2}	[2]
Ni/MoN/rNS	12h@640 mA cm^{-2}	[3]
$Co_{5.47}$/MoN@NF	80h@800 mA cm^{-2}	[4]
Rh, O-$MoSe_{2-x}$	100h@150 mA cm^{-2}	[5]
Ru/Mo_2C/MoO_2	100h@500 mA cm^{-2}	[6]
Ni_3Se_2@Ni500	190h@300 mA cm^{-2}	[7]
Ni_3Se_2-Ni600	300h@400 mA cm^{-2}	[8]
$Mose_2/Ni_3Se_2$-800	200h@800 mA cm^{-2}	This work

References

[1] X. Zheng, X. Wu, R. Wan, Y. Wang, B. Chen, G. Meng, Small **2025**, 2411696.

[2] D. Li, R. Wang, L. Yi, Y. Wei, J. Li, D. Zhao, W. Sun, W. Hu, Int. J. Hydrogen Energy **2024**, 49, 67-74.

[3] Y. Chen, Y. Wang, J. Yu, G. Xiong, H. Niu, Y. Li, D. Sun, X. Zhang, H. Liu, W. Zhou, Adv. Sci. **2022**, 9, 2105869.

[4] X. Shen, H. Li, T. Ma, Q. Jiao, Y. Zhao, H. Li, C. Feng, Small **2024**, 20, 2310535

[5] Z. Luo, Y. Guo, Y. Qian, L. Zhang, Z. Song, Q. Zhang, C. He, X. Ren, Adv. Funct. Mater. **2024**, 34, 2405881.

[6] L. Hou, C. Li, H. Jang, M. G. Kim, J. Z. Jiang, J. Cho, S. Liu, X. Liu, Adv. Mater. **2024**, 36, 2410039.

[7] M. M. Cui, Y. Zhao, B. Zhang, Z. L. Zhang, X. Q. Shi, J. B. Lai, K. N. Shan, S. Z. Wei, H. Pang, Int. J. Hydrogen Energy **2024**, 76, 181-189.

[8] Y. Zhao, M. Cui, B. Zhang, S. Wei, X. Shi, K. Shan, J. Ma, G. Zhou, H. Pang, Small Methods **2024**, 8, 2301465.